RSC Sustainability

ROYAL SOCIETY OF CHEMISTRY

PAPER

View Article Online
View Journal | View Issue

Cite this: *RSC Sustainability*, 2023, **1**, 1874

Visible-light driven fumarate synthesis from pyruvate and gaseous CO_2 with a hybrid system of photocatalytic NADH regeneration and dual biocatalysts†

Mika Takeuchi[a] and Yutaka Amao *[ab]

Fumarate is a useful unsaturated dicarboxylate utilized as a precursor for unsaturated polyester resin and biodegradable plastics. Fumarate is partially produced from petroleum-derived materials; thus, it is necessary to establish a synthesis from renewable raw materials such as gaseous CO_2 and biobased compounds with an external renewable energy source such as solar light. In this work, the visible-light driven synthesis of fumarate from biobased pyruvate is reported, which uses CO_2 directly captured from the gas phase by a 4-(2-hydroxyethyl)-1-piperazineethanesulfonic acid (HEPES)–NaOH buffer solution in combination with the NAD^+ reduction system of triethanolamine (TEOA), water-soluble zinc porphyrin, zinc *meso*-tetra(4-sulfonatophenyl) porphyrin tetrasodium salt (ZnTPPS) and the Rh coordination complex ($[Cp^*Rh(bpy)(H_2O)]^{2+}$; Cp^* = pentamethylcyclopentadienyl, bpy = 2,2′-bipyridyl). In addition, dual-biocatalysts consisting of malate dehydrogenase (oxaloacetate-decarboxylating; MDH; EC 1.1.1.38) from *Sulfobus tokodaii* and fumarase from porcine heart (FUM; EC 4.2.1.2) were used. It was found that pyruvate can be converted into L-malate with MDH by directly using CO_2 gas as a carboxylating agent in the presence of NADH. Moreover, the development of visible-light driven fumarate synthesis from gaseous CO_2 and pyruvate, employing a system with NADH regeneration and dual-biocatalysts as raw materials was also established.

Received 15th June 2023
Accepted 6th September 2023

DOI: 10.1039/d3su00194f

rsc.li/rscsus

Sustainability spotlight

This research focuses on synthesizing precursors for biodegradable polymers from gaseous CO_2 and biomass-derived molecules using visible-light energy and dual-biocatalysts in aqueous media under mild conditions compared with the conventional industrial method for the synthesis of precursors for biodegradable polymers. Therefore, this research contributes to CO_2 fixation and to alternative plastic precursor production for a more sustainable society. This system can fix gaseous CO_2 into organic molecules and convert it into high-value-added materials, resulting in long-term storage of CO_2 in molecules. This work aligns with the UN's Sustainable Development Goals, particularly Goal 7 "Affordable and Clean Energy" and 12 "Responsible Consumption and Production".

Introduction

Carbon capture utilization and sequestration (CCUS) technology aims to reduce CO_2 emissions. CCUS basically captures CO_2 released from power plants, factories, and fuel-burning industrial facilities and physically stores it geologically or converts it into useful materials.[1–5] In CCUS technologies, CO_2 can also be used as a raw material to produce C1 based fuels, chemicals, and polymers.[6] One key issue facing CCUS technologies is research and development of effective catalysts for CO_2 conversion into useful materials. Investigation and development of effective catalysts for converting CO_2 into useful materials is a pressing and important challenge in CCUS technology. Among the various catalysts, biocatalysts with the function of CO_2 conversion are also attracting a great deal of attention in CCUS technology. Biocatalysts with the function of CO_2 conversion are classified into two categories: those which reduce CO_2 to form C1 compounds such as CO or formate and those which build C–C bonds from CO_2 and organic molecules to produce carboxylate. CO_2, the final combustion product of carbohydrates, shows high stability but low reactivity, so external energy is required to convert it into useful materials.[7–12] Studies on visible light-driven CO_2 conversion systems, which hybridize a biocatalyst with a photoredox system consisting of a dye molecule or a photocatalyst and an electron mediator have been reported.[7,13–15] In particular, many studies have reported hybrid systems of formate dehydrogenase (FDH), which

[a]*Graduate School of Science, Osaka Metropolitan University, 3-3-138 Sugimoto, Sumiyoshi-ku, Osaka 558-8585, Japan*

[b]*Research Centre of Artificial Photosynthesis (ReCAP), Osaka Metropolitan University, 3-3-138 Sugimoto, Sumiyoshi-ku, Osaka 558-8585, Japan. E-mail: amao@omu.ac.jp*

† Electronic supplementary information (ESI) available. See DOI: https://doi.org/10.1039/d3su00194f

catalyzes the reduction of CO_2 to formate in the presence of NADH and photoredox systems.[16–31] On the other hand, visible-light driven CO_2 fixation to organic molecules has also garnered much attention in the research field of green chemistry.[7–12] For example, CO_2 as a feedstock is bound to an organic molecule as a carboxy-group based on building C–C bonds to produce a carboxylate. Malate dehydrogenase, decarboxylating (EC 1.1.1.39)[32,33] or oxaloacetate-decarboxylating (EC 1.1.1.40)[34,35] is an enzyme that catalyzes the reaction of decarboxylating L-malate into pyruvate and CO_2 and the reverse reaction of the introduced CO_2 as a carboxy-group to pyruvate to form L-malate in the presence of $NAD(P)^+$/NAD(P)H. Some studies on the visible-light driven L-malate production from pyruvate and bicarbonate with a system of an electron donor (D), a photosensitizer (P), methylviologen (MV) as an electron mediator, ferredoxin-$NADP^+$ reductase (FNR), $NAD(P)^+$ and MDH as shown in Fig. 1 have been reported.[36–38]

L-Malate is used in various applications in the food industry as an acidulant, pH adjuster and emulsifier. In contrast, poly(L-malic acid) (PMLA) polymerized with L-malate as a precursor (Fig. 2) has the outstanding features of biocompatibility, biodegradability, water solubility, and non-immunogenicity, and can be easily chemically modified.[39–44]

One candidate for the more effective use of L-malate synthesized from CO_2 is conversion to fumarate with a higher added value by intramolecular dehydration. Fumarate, an unsaturated dicarboxylic acid, is a chemical building block with many uses, including in the polymer industry.[45–49] In the field of polymer chemistry, fumarate is useful as a precursor for biodegradable plastic poly (butylene succinate) (PBS)[50] as shown in Fig. 2.

In the system shown in Fig. 1, visible light-driven regeneration of NAD(P)H was achieved. However, this system is very complicated. Moreover, FNR used in this system is a very expensive biological reagent. Thus, it is necessary to simplify it by using a novel catalyst instead of FNR for selective $NAD(P)^+$ reduction to NAD(P)H. The Rh complex ($[Cp^*Rh(bpy)(H_2O)]^{2+}$; Cp^* = pentamethylcyclopentadienyl, bpy = 2,2′-bipyridyl) and colloidal Rh nanoparticles are candidates for selective reduction of $NAD(P)^+$ to NAD(P)H.[51–55]

We previously reported biocatalytic fumarate production from bicarbonate and pyruvate *via* L-malate as an intermediate with two biocatalysts malate dehydrogenase (NAD^+-dependent oxaloacetate-decarboxylating; MDH EC 1.1.1.38) and fumarase (FUM; EC 4.2.1.2) in the presence of NADH in aqueous media, and the conversion yield for pyruvate to fumarate was estimated to be 14.4% after 25 h.[56,57] Since this system uses NADH as a sacrificial reagent, it is necessary to integrate the NAD^+ into NADH regeneration system. Thus, visible-light driven fumarate production from pyruvate and bicarbonate with the combination of NAD^+ reduction to the NADH system of triethanol amine (TEOA) as an electron donor, a water-soluble zinc porphyrin, zinc *meso*-tetra(4-sulfonatophenyl)porphyrin tetrasodium salt (ZnTPPS) as a photosensitizer and $[Cp^*Rh(bpy)(H_2O)]^{2+}$, as well as dual biocatalysts (MDH and FUM) has also been reported, as shown in Fig. 3.[58]

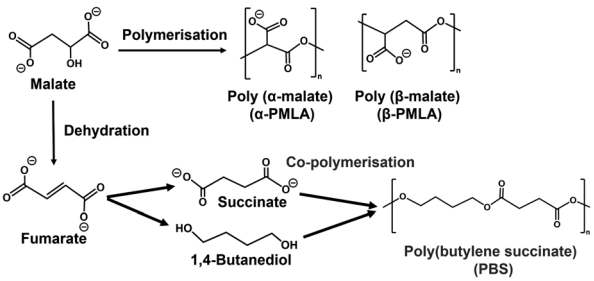

Fig. 2 Chemical structures of 3-hydroxybutyrate, poly-3-hydroxybutyrate (PHB) and poly (3-hydroxybutyrate)-*co*-(hydroxyvalerate) (PHB-*co*-PHV).

In this system, bicarbonate was used as a carboxylating agent for pyruvate instead of CO_2. For this reason, the MDH-catalyzed pyruvate carboxylation process requires bicarbonate.

Therefore, we devised the direct utilization of CO_2 gas instead of bicarbonate in the visible-light driven fumarate synthesis as a CO_2 capture and utilization (CCU) system, as shown in Fig. 3. One of the candidates for capturing gaseous CO_2 in an aqueous solution is a method using a basic aqueous solution containing amines. It was found that a pH of the reaction solution above pH 7.0 was optimal for the visible light-driven NADH regeneration in the system shown in Fig. 3. Furthermore, it was also reported that the enzymatic activities of MDH and FUM were optimal between pH 7.0 and 7.5 of the reaction solution. In other words, by using a weakly basic buffer such as 4-(2-hydroxyethyl)-1-piperazineethanesulfonic acid (HEPES)–NaOH solution in the system shown in Fig. 3, CO_2 in the gas phase can be directly captured and converted to bicarbonate.[59]

In this study, the visible-light driven fumarate synthesis from pyruvate and CO_2 directly captured from the gas phase by a HEPES–NaOH buffer solution with the combination of the NAD^+ reduction system of TEOA, ZnTPPS and $[Cp^*Rh(bpy)(H_2O)]^{2+}$, as well as MDH and FUM was investigated.

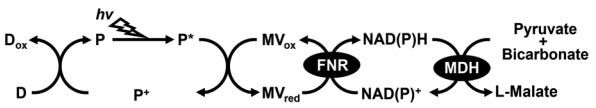

Fig. 1 Visible-light driven L-malate production from pyruvate and bicarbonate with the system of an electron donor (D), a photosensitizer (p), methylviologen oxidized form (MV_{ox}), FNR, $NAD(P)^+$ and MDH.

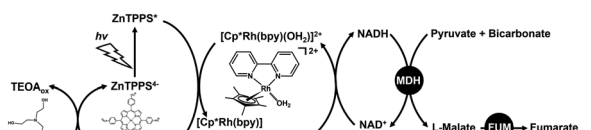

Fig. 3 Visible-light driven fumarate synthesis from pyruvate and bicarbonate with the combination of the NAD^+ reduction system of TEOA as an electron donor, ZnTPPS as a photosensitizer and $[Cp^*Rh(bpy)(H_2O)]^{2+}$, as well as dual biocatalysts consisting of MDH and FUM.

Experimental

Materials

NAD^+ and NADH were purchased from Oriental Yeast Co., Ltd. Sodium pyruvate, sodium bicarbonate, magnesium chloride hexahydrate and triethanolamine (TEOA) were purchased from FUJIFILM Wako Pure Chemical Corporation. (Pentamethylcyclopentadienyl) rhodium(III) dichloride dimer ($[Cp^*RhCl_2]_2$) and 2,2′-bipyridyl were purchased from Tokyo Chemical Industry Co., Ltd. Zinc *meso*-tetra(4-sulfonatophenyl) porphyrin tetrasodium salt (ZnTPPS) was purchased from Frontier Scientific Inc. 4-(2-Hydroxyethyl)-1-piperazineethanesulfonic acid (HEPES) was purchased from NACALAI TESQUE, INC. Malate dehydrogenase decarboxylating type (MDH, EC 1.1.1.38 code: MDH-73-01 was obtained from *Sulfobus tokodaii*; the commercially available reagent, 14 mg mL^{-1}; 0.55 units mg^{-1}) was purchased from Thermostable Enzyme Laboratory Co., Ltd. One activity unit of ME converted 1.0 μmol of NADH to NAD^+ in the presence of 10 mM sodium pyruvate, 0.3 mM NADH, 10 mM sodium bicarbonate and 10 mM magnesium chloride in 50 mM 1,4-piperazinediethanesulfonic acid–KOH buffer per min at pH 6.5 at 37 °C, according to the data sheet provided by Thermostable Enzyme Laboratory Co., Ltd. The molecular weight of ME was estimated to be 40 kDa based on the SDS-page using electrophoresis. Fumarase (FUM) from porcine heart (EC 4.2.1.2; molecular weight: 200 kDa)[60,61] was purchased from Merck Co., Ltd. One activity unit of FUM converted 1.0 μmol of L-malate to fumarate in potassium phosphate buffer per min at pH 7.6 at 25 °C.

Pentamethylcyclopentadienyl(2,2′-bipyridyl)rhodium(III) chloride ($[Cp^*Rh(bpy)(H_2O)]^{2+}$) was synthesized from $[Cp^*RhCl_2]_2$ and 2,2′-bipyridine according to a previous report.[62]

Estimation of the amount of CO_2 in the gas phase captured in a sample solution

The estimation method for CO_2 in the gas phase captured in the sample solution are as follows. The reaction is an isobaric system, as shown in Fig. 4.

The HEPES–NaOH buffer (500 mM; pH 7.8) was used as a sample solution. The sample solution was deaerated by freeze–pump–thaw cycles repeated 6 times and then flushed in the gas phase and syringed with the CO_2 gas. The total pressure was maintained at 1.01325×10^5 Pa. The volume change in the syringe was measured and the amount of CO_2 dissolved in the liquid phase was estimated. Here, CO_2 was regarded as a real gas, and the amount of CO_2 (n) in the gas phase was calculated using the following eqn (1).

$$\left(P + \frac{an^2}{V^2}\right)(V + nb) = nRT \quad (1)$$

Here, P is the initial pressure (1.01325×10^5 Pa). Symbols a and b are van der Waals coefficients ($a = 365 \times 10^{-3}$ Pa m^6 mol^{-2}; $b = 42.8 \times 10^{-6}$ m^3 mol^{-1}). V is the gas phase volume change in the syringe. T is the reaction temperature (303.65 K). R is the gas constant (8.31 J K^{-1} mol^{-1}). Symbol n is the amount of CO_2 (mol).

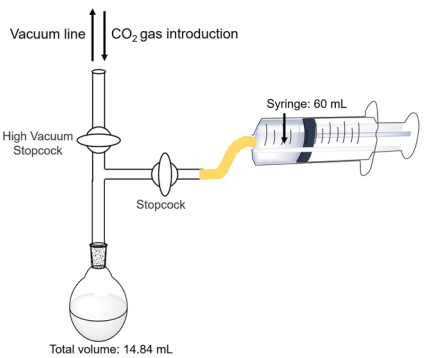

Fig. 4 Outline of the experimental setup for the estimation of the amount of CO_2 in the gas phase captured in a sample solution.

Kinetic parameters for L-malate production from pyruvate and bicarbonate with MDH in the presence of NADH

The reaction mixture consisted of sodium pyruvate (5.0 mM), magnesium chloride (10 mM), NADH (5.0 mM), sodium bicarbonate and MDH (0.7 U; *ca.* 1.6 μM) in 5.0 mL of 500 mM HEPES buffer–NaOH (pH 7.0). The concentration of sodium bicarbonate was varied from 0 to 100 mM. The amount of L-malate produced was detected by ion chromatography (Metrohm, Eco IC; electrical conductivity detector) with an ion exclusion column (Metrosep Organic Acids 250/7.8 Metrohm; column size: 7.8 × 250 mm; composed of 9 μm polystyrene–divinylbenzene copolymer with sulfonic acid groups). Details of pyruvate or L-malate quantification by ion chromatography are described in the ESI.† The pyruvate and L-malate concentration were determined from the calibration curve based on the chromatogram of a standard sample (Fig. S1 and S2†) using the eqn (S1) and (S2).† The concentration of L-malate production for 30 min was estimated as the initial rate.

L-Malate production from the pyruvate and directly captured CO_2 with MDH

The reaction mixture consisted of sodium pyruvate (5.0 mM), magnesium chloride (5.0 mM), NADH (5.0 mM) and MDH (0.7 U; *ca.* 1.6 μM) in 5.0 mL of 500 mM HEPES buffer–NaOH (pH 7.8). The reaction vessel is a clear glass vial (11.0 mL) and an isobaric system by feeding CO_2 gas into the vessel gas phase. The total pressure was maintained at 1.01325×10^5 Pa. The amount of pyruvate or L-malate was detected by ion chromatography.

Fumarate synthesis from the pyruvate and directly captured CO_2 with MDH and FUM

The reaction mixture consisted of sodium pyruvate (5.0 mM), magnesium chloride (5.0 mM), NADH (5.0 mM), MDH (0.7 U; 1.6 μM) and FUM (0.5 U; 1.3 nM) in 5.0 mL of 500 mM HEPES–NaOH buffer (pH 7.8). This reaction is also an isobaric system similar to the above. The total pressure was maintained at 1.01325×10^5 Pa. The concentrations of pyruvate, L-malate and

fumarate were detected by ion chromatography. The fumarate concentration was determined from the calibration curve based on the chromatogram of a standard sample (Fig. S3†) using the eqn (S3).†

Visible-light driven NAD^+ reduction to NADH with a system of TEOA, ZnTPPS and $[Cp^*Rh(bpy)(H_2O)]^{2+}$ under various pH conditions

The reaction mixture consisted of TEOA (0.2 M), ZnTPPS (10 μM), $[Cp^*Rh(bpy)(H_2O)]^{2+}$ (10 μM) and NAD^+ (0.5 mM) in 5.0 mL of 500 mM HEPES–NaOH buffer. The pH of the sample solution was varied from 6.4 to 8.1. The reaction is an isobaric system as shown in Fig. 5. The sample solution was deaerated by freeze–pump–thaw cycles repeated 6 times and then flushed in the gas phase with Ar gas for 10 min. The sample solution was irradiated with a 250 W halogen lamp (Panasonic) as a visible-light source (light intensity: 200 J m^{-2} s^{-1}) at 30 °C. The concentration of NADH was monitored by the absorption spectrum change using UV-visible absorption spectroscopy (SHIMADZU, MaltiSpec-1500) with the molar coefficient at 340 nm (ε = 6220 cm^{-1} M^{-1}).[63] The concentration of NADH production for 30 min was estimated as the initial rate.

Visible-light driven L-malate synthesis from pyruvate and direct capture of CO_2 with the system of TEOA, ZnTPPS, $[Cp^*Rh(bpy)(H_2O)]^{2+}$, NAD^+ and MDH

The reaction mixture consisted of sodium pyruvate (5.0 mM), magnesium chloride (5.0 mM), TEOA (0.2 M), ZnTPPS (10 μM), $[Cp^*Rh(bpy)(H_2O)]^{2+}$ (10 μM), NAD^+ (0.5 mM) and MDH (0.7 U; 1.6 μM) in 5.0 mL of 500 mM HEPES–NaOH buffer (pH 7.8). The sample solution was deaerated by freeze–pump–thaw cycles repeated 6 times and then flushed in the gas phase and a balloon with CO_2 gas for 10 min. The sample solution was irradiated with a 250 W halogen lamp as a visible-light source (light intensity: 200 J m^{-2} s^{-1}) at 30 °C. The reaction is also an isobaric system, as shown in Fig. 5. The total pressure was maintained at 1.01325×10^5 Pa. The concentration of L-malate was detected by ion chromatography using the eqn (S2).†

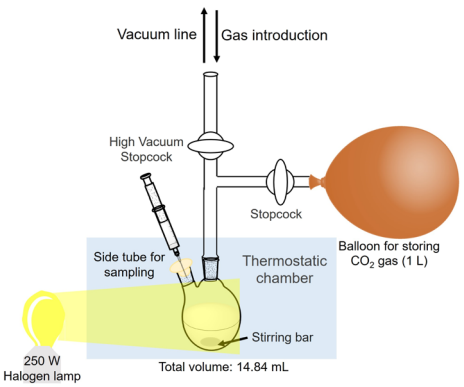

Fig. 5 Outline of the experimental setup of the isobaric system utilized for direct capture of CO_2 gas.

Visible-light driven fumarate synthesis from pyruvate and directly captured CO_2 with the system of TEOA, ZnTPPS, $[Cp^*Rh(bpy)(H_2O)]^{2+}$, NAD^+, MDH and FUM

The reaction mixture consisted of sodium pyruvate (5.0 mM), magnesium chloride (5.0 mM), TEOA (0.2 M), ZnTPPS (10 μM), $[Cp^*Rh(bpy)(H_2O)]^{2+}$ (10 μM), NAD^+ (0.5 mM), MDH (0.7 U; 1.6 μM) and FUM (0.5 U; 1.3 nM) in 5.0 mL of 500 mM HEPES–NaOH buffer (pH 7.8). The sample solution was deaerated by freeze–pump–thaw cycles repeated 6 times and then flushed in the gas phase and a balloon with the mixture gas of N_2 and CO_2 prepared in a mixing chamber for 10 min. The sample solution was irradiated with a 250 W halogen lamp (light intensity: 200 J m^{-2} s^{-1}) as a visible-light source at 30.5 °C. The reaction is also an isobaric system as shown in Fig. 5. The total pressure was maintained at 1.01325×10^5 Pa. The concentrations of L-malate and fumarate were detected by ion chromatography using the eqn (S2) and (S3).†

Results and discussion

Estimation of the capture of CO_2 in the gas phase into a sample solution

Fig. 6 shows the time dependence of the volume (ΔV) of the syringe of the experimental apparatus shown in Fig. 4. As shown in Fig. 6, the volume of the syringe decreased with increasing incubation time. Fig. 6 also shows the result of calculating the amount of CO_2 from the volume change of the syringe using eqn (1). In addition, it is predicted that CO_2 is more soluble in aqueous media more than pH 7. Therefore, the observed volume decrease is due to the dissolution of CO_2 gas into the buffer solution.

As shown in Fig. 6, the amount of CO_2 dissolved into the HEPES buffer solution was estimated to be *ca.* 0.7 mmol (*ca.* 140 mM in 5.0 mL of buffer solution). The results of this experiment indicated that CO_2 in the gas phase was captured in the sample solution over time by HEPES buffer. Here, CO_2 gas dissolves in aqueous media and then the hydrated CO_2 reacts

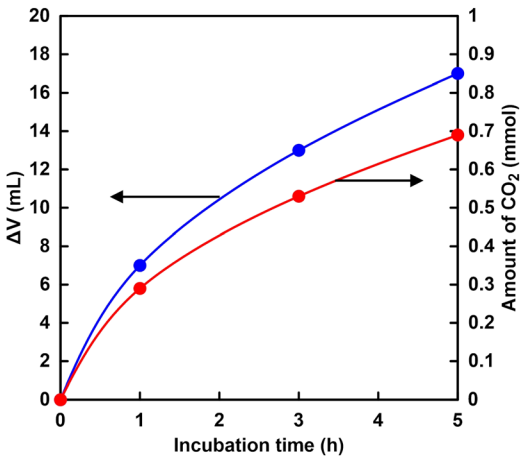

Fig. 6 Time dependence of the volume change (ΔV) of the syringe of the experimental apparatus (●) and calculating the amount of CO_2 from the volume change of the syringe (●).

with water to produce H_2CO_3. Dissociation of H_2CO_3 produces bicarbonate and carbonate depending on the pH of the solution, as shown in Fig. 7.[64]

The distribution ratio of CO_2 (aq) and bicarbonate were estimated to be *ca.* 18 and 82% at pH 7.0 calculated using the Plummer and Busenberg equation.[65] As shown in Fig. 6, the estimated CO_2 concentration was calculated to be 140 mM. Thus, the bicarbonate concentration was estimated to be 115 mM in the HEPES buffer solution (pH 7.0).

Next, the bicarbonate concentration required for the MDH catalytic reaction was determined by using Michaelis–Menten analysis and the possibility of using CO_2 gas captured into a sample solution from the gas phase as a raw material was also investigated. Fig. 8 shows the relationship between the sodium bicarbonate concentration and the initial rate for L-malate production with MDH (v_0). The v_0 was calculated from the concentration of L-malate production with MDH after 30 min incubation. As shown in Fig. 8, the v_0 was increased with increasing sodium bicarbonate concentration until 50 mM and then was saturated. The plot in Fig. 8 obeyed the Michaelis–Menten relationship. The Michaelis–Menten constant K_m and the maximum rate (V_{max}) of MDH for carboxylation of pyruvate with bicarbonate was estimated to be 14 mM and 0.03 mM min^{-1}. Therefore, it is estimated that the concentration of bicarbonate produced from CO_2 captured by HEPES from the gas phase into the sample solution has about 8.2 times the K_m of MDH.

In general, a substrate concentration three times higher than the K_m value is required for a stable enzymatic reaction. Thus, it was suggested that the bicarbonate captured from CO_2 gas could be used in MDH-catalyzed carboxylation of pyruvate L-malate production.

L-Malate synthesis from the pyruvate and directly captured CO_2 with MDH

Fig. 9 shows the time dependence of the concentration of pyruvate or L-malate with MDH in HEPES–NaOH buffer (the ion chromatograph chart during the reaction is shown in Fig. S4†).

The gas phase was filled with 100% CO_2. The L-malate concentration was increased with increasing incubation time. In contrast, the pyruvate concentration decreased with increasing incubation time. After 7 h incubation, the L-malate concentration was estimated to be 2.3 mM. The conversion yield for pyruvate to L-malate was estimated to be 46%. The initial reaction rate in this system was estimated to be 0.03 mM min^{-1}. On the other hand, the V_{max} of MDH for the carboxylation of pyruvate with bicarbonate was calculated to be 0.03 mM min^{-1} under the condition of 5.0 mM pyruvate from the result of Fig. 8. These results indicate that pyruvate is carboxylated using gaseous CO_2 as a starting material instead of bicarbonate.

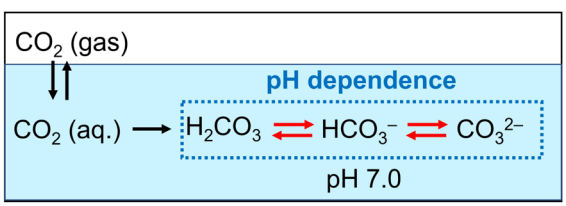

Fig. 7 Dissociation process of H_2CO_3 into bicarbonate and carbonate.

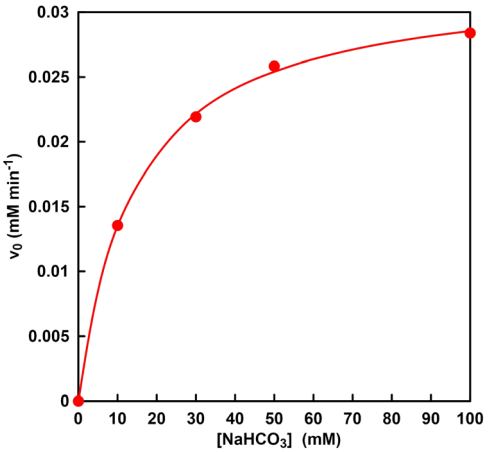

Fig. 8 Relationship between the sodium bicarbonate concentration and the initial rate for L-malate production with MDH (v_0).

Fumarate synthesis from the pyruvate and directly captured CO_2 with MDH and FUM

Fig. 10 shows the time dependence of the concentration of pyruvate, L-malate or fumarate with MDH and FUM in HEPES–NaOH buffer (the ion chromatograph chart during the reaction is shown in Fig. S5†). The gas phase was filled with 100% CO_2.

L-Malate and fumarate concentrations increased with incubation time. On the other hand, pyruvate concentration decreased with incubation time. After 7 h incubation, the concentration of fumarate produced was estimated to be 0.61 mM. The conversion yield for pyruvate to fumarate was estimated to be *ca.* 12% after 7 h incubation. On the other hand,

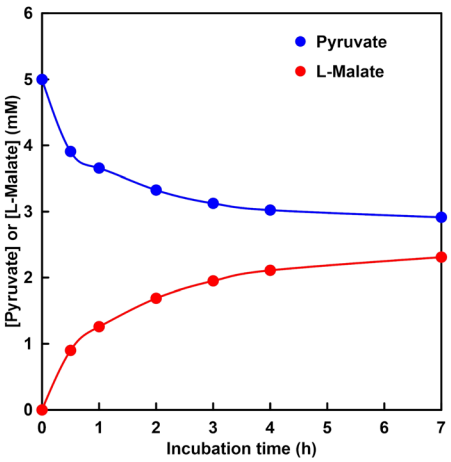

Fig. 9 Time dependence of pyruvate or L-malate concentration in the solution of sodium pyruvate (5.0 mM), magnesium chloride (5.0 mM), NADH (5.0 mM) and MDH (0.7 U, *ca.* 1.6 μM) in 5.0 mL of 500 mM HEPES–NaOH buffer (pH 7.8). The gas phase: CO_2.

in a fumarate synthesis system using sodium bicarbonate as a raw material under the same conditions, the concentration of fumarate produced and the conversion yield after 7 h incubation are reported to be 0.65 mM and *ca.* 13%, respectively. It was shown that there is no significant difference between the two systems. Thus, it shows that CO_2 in the gas phase can be used directly as a carboxylating agent for pyruvate instead of bicarbonate.

The pH dependence of visible-light driven NAD^+ reduction to NADH with the system of TEOA, ZnTPPS and $[Cp^*Rh(bpy)(H_2O)]^{2+}$

The NADH production rate is an important factor rather than the NADH accumulation concentration within a certain period of time in the visible-light driven fumarate or L-malate synthesis from pyruvate and gaseous CO_2. Fig. 11 shows the NADH production rate (v) in the system of TEOA, ZnTPPS and $[Cp^*Rh(bpy)(H_2O)]^{2+}$ under various pH conditions.

As shown in Fig. 11, it was found that the rate of NADH production increased with increasing the pH of the sample solution. This phenomenon is due to the ionization of the nitrogen atom of TEOA as an electron donor. Fig. 12 shows the single-electron transfer (SET) process from TEOA to the accepter molecule.

As shown in Fig. 12, $TEOA_{ox}$ is produced by releasing a single electron of the lone pair on the nitrogen atom of TEOA. Thus, it is suggested that the electron donating capability of $TEOAH^+$ without a lone pair on the nitrogen decreases. The pK_a of $TEOAH^+$ was reported to be 7.54 at 30 °C.[66] As the pH of the sample solution increased, thus, the distribution of TEOA increased, resulting in an increase in the NADH production rate. Although the visible-light driven reduction of NAD^+ depends on the pH of the sample solution, NADH was regenerated from NAD^+ by visible light irradiation even under neutral pH conditions, which is the optimal pH for MDH and FUM (pH 7.0–7.5). These results suggest that the visible-light driven reduction of the NAD^+ system is applicable to hybridize the dual-biocatalysts.

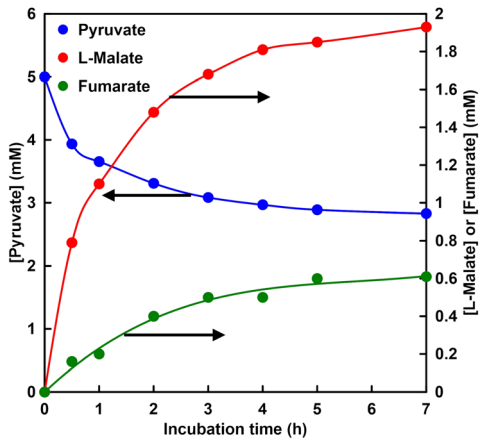

Fig. 10 Time dependence of pyruvate, L-malate or fumarate concentration in a solution of sodium pyruvate (5.0 mM), magnesium chloride (5.0 mM), NADH (5.0 mM), MDH (0.7 U, *ca.* 1.6 μM) and FUM (0.5 U; 1.3 nM) in 5.0 mL of 500 mM HEPES–NaOH buffer (pH 7.8). The gas phase: CO_2.

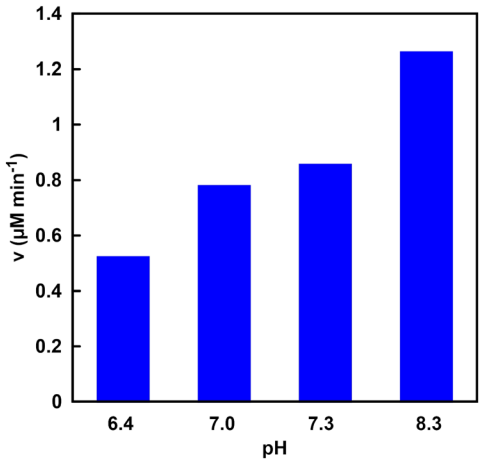

Fig. 11 Visible-light driven NADH production rate (v) in the system of TEOA, ZnTPPS and $[Cp^*Rh(bpy)(H_2O)]^{2+}$ under various pH conditions.

Visible-light driven L-malate synthesis from pyruvate and directly captured CO_2 with the system of TEOA, ZnTPPS, $[Cp^*Rh(bpy)(H_2O)]^{2+}$, NAD^+ and MDH

The visible-light driven L-malate synthesis from pyruvate and bicarbonate with the system of sodium pyruvate, magnesium chloride, TEOA, ZnTPPS, $[Cp^*Rh(bpy)(H_2O)]^{2+}$, NAD^+, and MDH has been reported previously. Therefore, utilization of directly captured CO_2 gas instead of bicarbonate in this system was investigated. Fig. 13 shows the time dependence of L-malate concentration in the sample solution of sodium pyruvate, magnesium chloride, TEOA, ZnTPPS, $[Cp^*Rh(bpy)(H_2O)]^{2+}$, NAD^+, and MDH under irradiation (the ion chromatography chart during the reaction is shown in Fig. S6†). The gas phase was filled with CO_2 gas. Fig. 13 also shows the time dependence of the L-malate concentration in the sample solution of sodium pyruvate, magnesium chloride, TEOA, ZnTPPS, $[Cp^*Rh(bpy)(H_2O)]^{2+}$, NAD^+, sodium bicarbonate and MDH under irradiation. In this system, the gas phase was also filled with CO_2 gas.

As shown in Fig. 13, L-malate concentration increased constantly over the irradiation time and 157 μM of L-malate was produced after 5 h. This linear increase in L-malate over the irradiation time indicates that bicarbonate was captured from

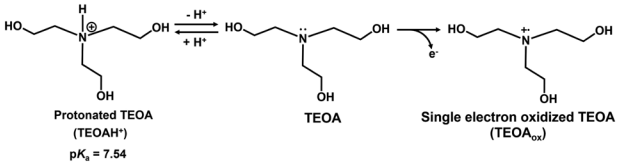

Fig. 12 The relationship between protonated TEOA ($TEOAH^+$) and TEOA, and the single-electron oxidation process to produce $TEOA_{ox}$.

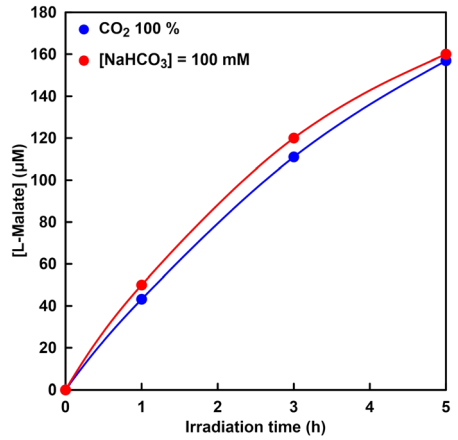

Fig. 13 Time dependence of L-malate concentration in a solution of sodium pyruvate (5.0 mM), magnesium chloride (5.0 mM), TEOA (0.2 M), ZnTPPS (10 μM), $[Cp^*Rh(bpy)(H_2O)]^{2+}$ (10 μM), NAD^+(0.5 mM) and MDH (0.7 U, *ca.* 1.6 μM) in 5 mL of 500 mM HEPES–NaOH buffer (pH 7.8) under irradiation. ●: gas phase: CO_2 gas; ●: $[NaHCO_3] = 100$ mM, gas phase: CO_2 gas.

CO_2 gas continuously and fixed to pyruvate with MDH in the presence of NADH produced by visible light irradiation. As shown in Fig. 13, it was shown that there is no significant difference between the systems using bicarbonate and CO_2 gas as a carboxylating agent for pyruvate. In addition, the catalytic turnover number of MDH in the visible-light driven L-malate synthesis was estimated to be 100, suggesting that CO_2 fixation to pyruvate proceeded effectively with MDH. From these results, it can also be seen that CO_2 in the gas-phase can be used directly as a carboxylating agent for pyruvate instead of bicarbonate in the visible-light driven L-malate synthesis. However, compared to the system using NADH as a sacrificial reagent, as shown in Fig. 9, the efficiency of the visible light-driven L-malate synthesis is low. This is presumed to be due to the slow visible light reduction rate of NAD^+ in the system of TEOA, ZnTPPS, and $[Cp^*Rh(bpy)(H_2O)]^{2+}$.

Visible-light driven fumarate synthesis from pyruvate and directly captured CO_2 with the system of TEOA, ZnTPPS, $[Cp^*Rh(bpy)(H_2O)]^{2+}$, NAD^+, MDH and FUM

Finally, visible-light driven fumarate synthesis from pyruvate and directly captured CO_2 with the system of TEOA, ZnTPPS, $[Cp^*Rh(bpy)(H_2O)]^{2+}$, NAD^+, MDH and FUM was investigated.

Fig. 14 shows the time dependence of L-malate (a) and fumarate (b) concentration in the sample solution of sodium pyruvate, magnesium chloride, TEOA, ZnTPPS, $[Cp^*Rh(bpy)(H_2O)]^{2+}$, NAD^+, MDH and FUM with a mixed gas with different mixing ratios of CO_2 and N_2 under irradiation (the ion chromatography chart during the reaction is shown in Fig. S7†). As shown in Fig. 14, the L-malate and fumarate concentrations increase with the irradiation time under all conditions. It was clarified that concentration of visible-light driven fumarate synthesis depends on CO_2 gas concentration in the gas phase. No significant difference in fumarate synthesis was observed under 100% CO_2 in the gas phase and the presence of sodium

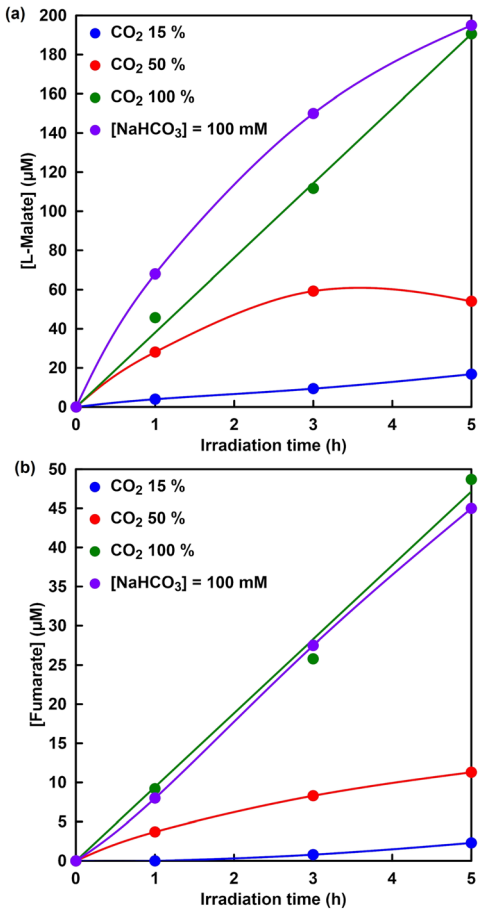

Fig. 14 Time dependence of L-malate (a) or fumarate (b) concentration in the solution of sodium pyruvate (5.0 mM), magnesium chloride (5.0 mM), TEOA (0.2 M), ZnTPPS (10 μM), $[Cp^*Rh(bpy)(H_2O)]^{2+}$ (10 μM), NAD^+(0.5 mM), MDH (0.7 U, *ca.* 1.6 μM) and FUM (0.5 U; 1.3 nM) in 5 mL of 500 mM HEPES–NaOH buffer (pH 7.8) under conditions with varying ratios of CO_2 and N_2 in the gas phase with irradiation.

bicarbonate conditions. On the other hand, the synthesis of L-malate and fumarate with the visible-light driven system decreased under the conditions of CO_2 concentration of 50 or 15% in the gas phase. The first step in the visible-light driven fumarate synthesis, the dissolution process of CO_2, requires a supply of bicarbonate, which is necessary for the MDH-catalyzed carboxylation of pyruvate to produce L-malate. As shown in Fig. 14, under the conditions of a CO_2 concentration of 50 or 15%, not only fumarate synthesis but also L-malate synthesis greatly depends on the gas-phase CO_2 concentration. Thus, it is proposed that the low concentration of L-malate synthesis is due to the low CO_2 gas concentration in the gas phase and the slow dissolution rate in the reaction solution. Next, let us compare L-malate synthesis in the visible-light driven fumarate synthesis under 100% CO_2 in the gas phase and the presence of sodium bicarbonate conditions. Under the presence of sodium bicarbonate conditions, the initial rate of L-malate synthesis in the visible-light driven fumarate synthesis is higher than that under 100% CO_2 in the gas phase condition. This is presumed to be due to the fact that the MDH-catalyzed carboxylation of

pyruvate under the condition of 100% CO_2 involves the dissolution of CO_2 in the gas phase into the reaction solution and the production of bicarbonate. On the other hand, there was no significant difference between under 100% CO_2 in the gas phase and the presence of sodium bicarbonate conditions in the FUM-catalyzed fumarate synthesis. After 5 h irradiation, moreover, the ratios of L-malate and fumarate production concentrations under 15, 50 and 100% CO_2 in the gas phase are estimated to be 0.14, 0.29 and 0.26, respectively. These results suggest that the rate-limiting step in the overall reaction system is fumarate synthesis based on FUM-catalyzed dehydration of L-malate. Thus, CO_2 could be directly used as a raw material without using bicarbonate, because of CO_2 in the gas-phase trapping function of the HEPES buffer solution used in the reaction. Additionally, the captured CO_2 was converted to bicarbonate in the HEPES buffer and acted as a carboxylating agent for pyruvate with MDH. In order to improve fumarate synthesis efficiency, it is necessary to investigate the effect of each reaction element in the visible-light driven system on FUM catalytic activity.

Conclusions

In conclusion, we have demonstrated visible-light driven fumarate synthesis from pyruvate and CO_2 captured from the gas phase using HEPES–NaOH buffer solution with the combination of the NAD^+ reduction system of TEOA, ZnTPPS and $[Cp^*Rh(bpy)(H_2O)]^{2+}$, as well as dual biocatalysts of MDH and FUM without any bicarbonate. It was shown that pyruvate can be converted into L-malate with MDH by directly using CO_2 gas as a carboxylating agent in the presence of NADH. Moreover, the development of the visible light-driven fumarate synthesis from gaseous CO_2 and biobased pyruvate as raw materials with the combination of a NAD^+ reduction system of TEOA, ZnTPPS and $[Cp^*Rh(bpy)(H_2O)]^{2+}$, as well as dual biocatalysts of MDH and FUM was accomplished. Notably, no significant difference was observed between under 100% CO_2 in the gas phase and the presence of sodium bicarbonate conditions as a raw material in the visible light-driven fumarate synthesis. This system is the first example of achieving direct gaseous CO_2 fixation into pyruvate using the electron accumulation in NAD^+ with visible-light energy.

Conflicts of interest

There are no conflicts to declare.

Acknowledgements

This work was partially supported by Grant-in-Aid for Scientific Research (B) (22H01872) and (22H01871), the Fund for the Promotion of Joint International Research (Fostering Joint International Research (B)) (19KK0144), and by the Institute for Fermentation, Osaka (IFO) (G-2023-3-050).

Notes and references

1 A. Abdulla, R. Hanna, K. R. Schell, O. Babacanand and D. G. Victor, *Environ. Res. Lett.*, 2020, **16**, 014036.
2 N. Mac Dowell, N. Florin, A. Buchard, J. Hallett, A. Galindo, G. Jackson, C. S. Adjiman, C. K. Williams, N. Shah and P. Fennell, *Energy Environ. Sci.*, 2010, **3**, 1645.
3 M. Bui, C. S. Adjiman, A. Bardow, E. J. Anthony, A. Boston, S. Brown, P. S. Fennell, S. Fuss, A. Galindo, L. A. Hackett, J. P. Hallett, H. J. Herzog, G. Jackson, J. Kemper, S. Krevor, G. C. Maitland, M. Matuszewski, I. S. Metcalfe, C. Petit, G. Puxty, J. Reimer, D. M. Reiner, E. S. Rubin, S. A. Scott, N. Shah, B. Smit, J. P. M. Trusler, P. Webley, J. Wilcox and N. M. Dowell, *Energy Environ. Sci.*, 2018, **11**, 1062.
4 GCCSI, *Large-scale CCS Projects*, Global CCS Institute, **http://www.globalccsinstitute.com/projects/large-scale-ccs-projects**, accessed July 2017.
5 BEIS, *UK Carbon Capture and Storage: Government Funding and Support*, Department for Business, Energy & Industrial Strategy (BEIS), London, UK, **https://www.gov.uk/guidance/uk-carbon-capture-and-storage-government-funding-and-support**, accessed June 2017.
6 Nova-Institute, *Bio-based Building Blocks and Polymers*, Hurth (Germany), 2019.
7 T. Katagiri and Y. Amao, *Green Chem.*, 2020, **22**, 6682.
8 L. Yuan, M. Y. Qi, Z. R. Tang and Y. J. Xu, *Angew. Chem., Int. Ed.*, 2021, **60**, 21150.
9 C. Han, Y. H. Li, J. Y. Li, M. Y. Qi, Z. R. Tang and Y. J. Xu, *Angew. Chem., Int. Ed.*, 2021, **60**, 7962.
10 F. Zhang, Y. H. Li, M. Y. Qi, Y. M. A. Yamada, M. Anpo, Z. R. Tang and Y. J. Xu, *Chem Catal.*, 2021, **1**, 272.
11 J. Y. Li, L. Yuan, S. H. Li, Z. R. Tang and Y. J. Xu, *J. Mater. Chem. A*, 2019, **7**, 8676.
12 K. Q. Lu, Y. H. Li, F. Zhang, M. Y. Qi, X. Chen, Z. R. Tang, Y. M. A. Yamada, M. Anpo, M. Conte and Y. J. Xu, *Nat. Commun.*, 2020, **11**, 5181.
13 Y. Amao, *Sustainable Energy Fuels*, 2018, **2**, 1928.
14 Y. Amao, *Chem. Lett.*, 2017, **46**, 780.
15 Y. Amao, *J. CO2 Util.*, 2018, **26**, 623.
16 D. Mandler and I. Willner, *J. Chem. Soc., Perkin Trans. 2*, 1988, 997.
17 I. Willner and D. Mandler, *J. Am. Chem. Soc.*, 1989, **111**, 1330.
18 I. Willner, N. Lapidot, A. Riklin, R. Kasher, E. Zahavy and E. Katz, *J. Am. Chem. Soc.*, 1994, **116**, 1428.
19 I. Willner, I. Willner and N. Lapidot, *J. Am. Chem. Soc.*, 1990, **112**, 6438.
20 R. Miyatani and Y. Amao, *Biotechnol. Lett.*, 2002, **24**, 1931.
21 R. Miyatani and Y. Amao, *J. Mol. Catal. B: Enzym.*, 2004, **27**, 121.
22 R. Miyatani and Y. Amao, *J. Jpn. Pet. Inst.*, 2004, **47**, 27.
23 Y. Amao, R. Abe and S. Shiotani, *J. Photochem. Photobiol., A*, 2015, **313**, 149.
24 I. Tsujisho, M. Toyoda and Y. Amao, *Catal. Commun.*, 2006, **7**, 173.
25 M. Kodaka and Y. Kubota, *J. Chem. Soc., Perkin Trans. 2*, 1999, 891.
26 A. Miyaji and Y. Amao, *New J. Chem.*, 2021, **45**, 5780.
27 A. Miyaji and Y. Amao, *ChemNanoMat*, 2021, **7**, 626.
28 R. K. Yadav, G. H. Oh, N.-J. Park, A. Kumar, K. J. Kong and J. O. Baeg, *J. Am. Chem. Soc.*, 2014, **136**, 16728.

29 R. K. Yadav, J. O. Baeg, G. H. Oh, N. J. Park, K. J. Kong, J. Kim, D. W. Hwang and S. K. Biswas, *J. Am. Chem. Soc.*, 2012, **134**, 11455.
30 W. S. Choi, S. H. Lee, J. W. Ko and C. B. Park, *ChemSusChem*, 2016, **9**, 1559.
31 S. K. Kuk, R. K. Singh, D. H. Nam, R. Singh, J. K. Lee and C. B. Park, *Angew. Chem., Int. Ed.*, 2017, **129**, 3885.
32 J. A. Milne and R. A. Cook, *Biochemistry*, 1979, **18**, 3605.
33 M. A. Tronconi, M. C. Gerrard Wheeler, V. G. Maurino, M. F. Drincovich and C. S. Andreo, *Biochem. J.*, 2010, **430**, 295.
34 Z. Fu, Z. Zhang, Z. Liu, X. Hu and P. Xu, *Biol. Plant.*, 2011, **55**, 196.
35 Y. Wang, S. P. Long and X. G. Zhu, *Plant Physiol.*, 2014, **164**, 2231.
36 Y. Amao and M. Ishikawa, *J. Jpn. Pet. Inst.*, 2007, **50**, 272.
37 Y. Amao and M. Ishikawa, *Catal. Commun.*, 2007, **8**, 423.
38 T. Itoh, H. Asada, K. Tobioka, Y. Kodera, A. Matsushima, M. Hiroto, H. Nishimura, T. Kamachi, I. Okura and Y. Inada, *Bioconjugate Chem.*, 2000, **11**, 8.
39 E. Holler, B. Angerer, G. Achhammer, S. Miller and C. Windisch, *FEMS Microbiol. Rev.*, 1992, **9**, 109.
40 S. J. Liu and A. Steinbuchel, *Biotechnol. Lett.*, 1997, **19**, 11.
41 J. A. P. Arias, M. G. Alvarez, A. M. de Ilarduya, E. Holler, J. A. Galbis and S. M. Guerra, *Macromol. Biosci.*, 2008, **8**, 540.
42 M. Vert, *Polym. Degrad. Stab.*, 1998, **59**, 169.
43 B. S. Lee, M. Fujita, N. M. Khazenzon, K. A. Wawrowsky, S. Wachsmann-Hogiu, D. L. Farkas, K. L. Black, J. Y. Ljubimova and E. Holler, *Bioconjugate Chem.*, 2006, **17**, 317.
44 B. He, E. Wan and M. B. Chan-Park, *Chem. Mater.*, 2006, **18**, 3946.
45 B. D. Ahn, S. H. Kim, Y. H. Kim and J. S. Yang, *J. Appl. Polym. Sci.*, 2001, **82**, 2808.
46 I. Bechthold, K. Bretz, S. Kabasci, R. Kopitzky and A. Springer, *Chem. Eng. Technol.*, 2008, **31**, 647.
47 Y. Jiang, A. J. J. Woortman, G. O. R. Alberda van Ekenstein and K. Loos, *Polym. Chem.*, 2015, **6**, 5451.
48 A. Pellis, A. E. Herrero, L. Gardossi, V. Ferrario and G. M. Guebitz, *Polym. Int.*, 2016, **65**, 861.
49 N. A. Rorrer, J. R. Dorgan, D. R. Vardon, C. R. Martinez, Y. Yang and G. T. Beckham, *ACS Sustainable Chem. Eng.*, 2016, **4**, 6867.
50 N. Jacquel, F. Freyermouth, F. Fenouillot, A. Rousseau, J. P. Pascault, P. Fuertes and R. Saint-Loup, *J. Polym. Sci., Part A: Polym. Chem.*, 2011, **49**, 5301.
51 R. Ruppert, S. Herrmann and E. Steckhan, *Tetrahedron Lett.*, 1987, **28**, 6583.
52 E. Steckhan, S. Herrmann, R. Ruppert, J. Thömmes and C. Wandrey, *Angew. Chem., Int. Ed. Engl.*, 1990, **29**, 388.
53 H. C. Lo, O. Buriez, J. B. Kerr and R. H. Fish, *Angew. Chem., Int. Ed.*, 1999, **38**, 1429.
54 H. C. Lo, C. Leiva, O. Buriez, J. B. Kerr, M. M. Olmstead and R. H. Fish, *Inorg. Chem.*, 2001, **40**, 6705.
55 C. L. Pitman, O. N. L. Finster and A. J. M. Miller, *Chem. Commun.*, 2016, **52**, 9105.
56 M. Takeuchi and Y. Amao, *React. Chem. Eng.*, 2022, **7**, 1931.
57 M. Takeuchi and Y. Amao, *RSC Sustainability*, 2023, **1**, 90.
58 M. Takeuchi and Y. Amao, *Sustainable Energy Fuels*, 2023, **7**, 355.
59 Y. Kita and Y. Amao, *Green Chem.*, 2023, **25**, 2699.
60 J. C. Sacchettini, M. W. Frazier, D. C. Chiara, L. J. Banaszak and G. A. Grant, *Biochem. Biophys. Res. Commun.*, 1988, **153**, 435.
61 S. Beeckmans and E. Van Driessche, *J. Biol. Chem.*, 1998, **273**, 31661.
62 U. Kölle, B. S. Kang, P. Infelta, P. Comte and M. Grätzel, *Chem. Ber.*, 1989, **122**, 1869.
63 R. B. McComb, L. W. Bond, R. W. Burnett, R. C. Keech and G. N. Bowers Jr, *Clin. Chem.*, 1976, **22**, 141.
64 K. Teramura, K. Hori, Y. Terao, Z. Huang, S. Iguchi, Z. Wang, H. Asakura, S. Hosokawa and T. Tanaka, *J. Phys. Chem. C*, 2017, **121**, 8711.
65 L. N. Plummer and E. Busenberg, *Geochim. Cosmochim. Acta*, 1982, **46**, 1011.
66 M. R. Simond, *J. Solution Chem.*, 2012, **41**, 130.